Stem Cell Reports
Report
OPEN ACCESS

Pattern of Functional TTX-Resistant Sodium Channels Reveals a Developmental Stage of Human iPSC- and ESC-Derived Nociceptors

Esther Eberhardt,[1,2,9] Steven Havlicek,[3,7,9] Diana Schmidt,[1,3,9] Andrea S. Link,[1] Cristian Neacsu,[1] Zacharias Kohl,[4] Martin Hampl,[1,5] Andreas M. Kist,[1,8] Alexandra Klinger,[1] Carla Nau,[6] Jürgen Schüttler,[2] Christian Alzheimer,[1] Jürgen Winkler,[4] Barbara Namer,[1] Beate Winner,[3,*] and Angelika Lampert[1,5,*]

[1]Institute of Physiology and Pathophysiology, Friedrich-Alexander-Universität Erlangen-Nürnberg, Universitätsstraße 17, 91054 Erlangen, Germany
[2]Department of Anesthesiology, Universitätsklinikum Erlangen, Friedrich-Alexander-Universität Erlangen-Nürnberg, Krankenhausstrasse 12, 91054 Erlangen, Germany
[3]IZKF Junior Research Group and BMBF Research Group Neuroscience, IZKF, Friedrich-Alexander-Universität Erlangen-Nürnberg, Glückstrasse 6, 91054 Erlangen, Germany
[4]Department of Molecular Neurology, Universitätsklinikum Erlangen, Friedrich-Alexander-Universität Erlangen-Nürnberg, Schwabachanlage 6, 91054 Erlangen, Germany
[5]Institute of Physiology, Uniklinik RWTH Aachen, Pauwelsstrasse 30, 52074 Aachen, Germany
[6]Department of Anesthesiology and Intensive Care, University Medical Center Schleswig-Holstein, Campus Luebeck, Ratzeburger Allee 160, 23538 Lübeck, Germany
[7]Present address: Stem Cell & Regenerative Biology, Genome Institute of Singapore, A*STAR, 60 Biopolis Street, Singapore 138672, Singapore
[8]Present address: Max-Planck-Institute of Neurobiology, Am Klopferspitz 18, 82152 Martinsried, Germany
[9]Co-first author
*Correspondence: beate.winner@med.uni-erlangen.de (B.W.), alampert@ukaachen.de (A.L.)
http://dx.doi.org/10.1016/j.stemcr.2015.07.010

SUMMARY

Human pluripotent stem cells (hPSCs) offer the opportunity to generate neuronal cells, including nociceptors. Using a chemical-based approach, we generated nociceptive sensory neurons from HUES6 embryonic stem cells and retrovirally reprogrammed induced hPSCs derived from fibroblasts. The nociceptive neurons expressed respective markers and showed tetrodotoxin-sensitive (TTXs) and -resistant (TTXr) voltage-gated sodium currents in patch-clamp experiments. In contrast to their counterparts from rodent dorsal root ganglia, TTXr currents of hPSC-derived nociceptors unexpectedly displayed a significantly more hyperpolarized voltage dependence of activation and fast inactivation. This apparent discrepancy is most likely due to a substantial expression of the developmentally important sodium channel NAV1.5. In view of the obstacles to recapitulate neuropathic pain in animal models, our data advance hPSC-derived nociceptors as a better model to study developmental and pathogenetic processes in human nociceptive neurons and to develop more specific small molecules to attenuate pain.

INTRODUCTION

Human pluripotent stem cells (hPSCs), i.e., human embryonic stem cells (hESCs) and human induced pluripotent stem cells (hiPSCs), can give rise to functional neurons (reviewed in Gage and Temple, 2013). Human peripheral neurons are difficult to differentiate, but a recently published combinatorial small molecule-based approach was able to overcome this shortage (Chambers et al., 2012). These neurons express canonical markers of nociceptors, such as *TAC1* (pro-peptide to Substance P), *SCN9A* (NAV1.7), and *SCN10A* (NAV1.8). They exhibit currents mediated by ASIC, $GABA_A$ receptors, HCN1, and KCNQ2/3 (Young et al., 2014).

Neuropathic pain is a disabling and difficult to treat condition that cannot be adequately mimicked in animal models. Recently, inherited neuropathic pain syndromes were linked to mutations in voltage-gated sodium channels (NAVs) (Lampert et al., 2014), stressing the importance of TTXr NAVs in neuropathic pain and as targets for novel, specific pain treatment (Bagal et al., 2014).

Nociceptive stimuli are conveyed by NAVs that comprise nine different subtypes expressed in human and rodents. Six are tetrodotoxin-sensitive (TTXs) (NAV1.1 to NAV1.4, NAV1.6, and NAV1.7), whereas three are resistant to TTX (TTXr) (NAV1.5, NAV1.8, and NAV1.9). Inherited small fiber neuropathies (SFN) are, among others, associated with mutations in NAV1.8 (Faber et al., 2012). NAVs undergo expression changes during development, and pain syndromes linked to NAV mutations occur at certain periods in life; while the NAV1.7-linked severe pain syndrome PEPD (paroxysmal extreme pain disorder) can start in utero, with symptoms declining during adulthood, the NAV1.7-linked erythromelalgia has its onset in adolescence, and SFN is observed in older adults (Lampert et al., 2014). This striking variation in disease onset may be due to modulation of the mutation phenotypes by co-expression of different NAV subtypes, but experimental support for this hypothesis is still missing. Expression and function of NAVs depend critically on the cellular background (Rush et al., 2006), sounding a strong note of caution when translating data from rodent to human. This holds particularly

true for nociceptors whose excitability is controlled by a complex interplay between TTXs and TTXr NAVs. Thus, there is an urgent need for the availability of human nociceptors to investigate the pathophysiology and pharmacology of nociception in an appropriate model.

Even though hPSC-derived nociceptors are a promising cellular model in pain research, a detailed investigation of their set of NAV subtypes is still missing. Using hPSC-derived nociceptors, generated by applying an optimized protocol (Chambers et al., 2012), we explored the maturational stages of hPSC-derived nociceptors and deciphered the electrophysiological characteristics of their TTXr NAVs. Our analysis revealed that the generated neurons not only express NAV1.8 and NAV1.9, but also the developmentally regulated NAV1.5, suggesting that the derived neurons represent a specific stage during development.

RESULTS AND DISCUSSION

hPSC-Derived Sensory Neurons Express Key Nociceptor Markers

Using an optimized protocol for small molecule inhibition (Figure 1A), gained by adapting growth factor concentrations, antioxidant supplementation, and optimized cell seeding densities of a previously published protocol (Chambers et al., 2012), we successfully differentiated hESCs (HUES6 line) and hiPSCs (previously published as control lines iPSC Ctrl-11 and Ctrl-12) (Havlicek et al., 2014) into human sensory neurons. The reproducibility of the relative amount of nociceptors and reduced intraline variation were obtained when adjusting cell seeding densities to 85,000–100,000 cells/cm^2 (compared with 20,000–40,000 cells/cm^2 in Chambers et al., 2012), lowering the neurotrophic factor concentrations to 20 ng/ml, and supplementing the medium with the antioxidant ascorbic acid.

The generated neurons grow in ganglion-like clusters (Figure 1B) comparable to those of other mammalian sensory neurons (e.g., rat dorsal root ganglion neurons [DRGs]). Immunofluorescence stainings indicated the expression of canonical peripheral markers, such as BRN3A, PERIPHERIN, and TUJ1 (Figures 1C and 1D). The expression of the nociceptor-specific capsaicin receptor TRPV1 (Figure 1E) revealed that the majority of TUJ1-positive cells harbored nociceptor identity (83% of TUJ1-positive cells within ganglion-like clusters were TRPV1 positive). Compared with undifferentiated hiPSCs, the pan-neuronal NAVs NAV1.1, NAV1.2 and NAV1.6 (corresponding to genes *SCN1A*, *SCN2A*, and *SCN8A*) were upregulated in nociceptors (Figure 1F), indicating the successful differentiation into neuronal cells (Catterall et al., 2005). The expression of genes specific for peripheral sensory neurons such as NAV1.7 (*SCN9A*), the P_2X_3 receptor (*P2RX3*), and *TRPV1* were upregulated in the differentiated nociceptors compared with hiPSCs (Figure 1G).

For performing a functional analysis, we tested neuronal excitability by whole-cell patch-clamp experiments. When electrically evoked, hPSC-derived nociceptors fired tonically (9 of 29) or phasically (15 of 29) as described for rodent sensory neurons (Figure 1H; e.g., Freisinger et al., 2013), and only few cells were not electrically active (5 of 29). Consecutive voltage clamp recordings of each cell revealed the characteristic ionic signature of neuronal excitability, with brief NAV-mediated inward currents followed by sustained outward currents (Figure 1I). TTX (500 nM) was used to delineate TTXr NAVs in hPSC-derived nociceptors, for which a sample recording is shown in Figure 1J.

TTXr Currents in hPSC-Derived Nociceptors

Of the three known TTXr NAVs, NAV1.8 and NAV1.9 are expressed in the peripheral nervous system, and NAV1.5 is mainly present in the heart (Catterall, 2012). However, NAV1.5 is also found in rat DRGs during development (Renganathan et al., 2002). We therefore compared expression levels of NAV1.5, NAV1.8, and NAV1.9 in hPSC-derived nociceptors (Figure 2A). Undifferentiated hiPSCs already showed substantial expression of *SCN5A*, suggesting that this channel may play a role during early human development. Upon differentiation of hiPSCs into nociceptors, *SCN5A* remained present, indicating its importance for sensory neuron development. We found a substantial increase in *SCN10A* (encoding NAV1.8) and *SCN11A*, encoding the slowly gating NAV1.9, confirming that the differentiated cells acquired a peripheral neuron identity. The abundance of NAV1.5 and NAV1.9 protein was confirmed by immunofluorescence stainings (Figure 2B). We evaluated several NAV1.8 antibodies; however, all failed to be specific in heterologous expression systems (data not shown).

We explored whether TTXr NAVs of hPSC-derived nociceptors display the distinct biophysical characteristics. In whole-cell recordings performed in the presence of 500 nM TTX, 79% of cells displayed substantial fast TTXr NAV currents with properties similar to those of human NAV1.8 when heterologously expressed in the neuroblastoma cell line ND7/23 (Figure 2C). We focused on fast-gating NAVs, as currents resembling NAV1.9 were only weakly expressed (data not shown). Compared with heterologously expressed NAV1.8, voltage dependence of activation was much more hyperpolarized in human nociceptors (Figure 2D), suggesting that either NAV1.8 displays different gating properties in human nociceptors or that other NAVs were also involved. In support of the latter, the voltage dependence of activation of hPSC-derived nociceptors was indeed more similar to that of heterologously

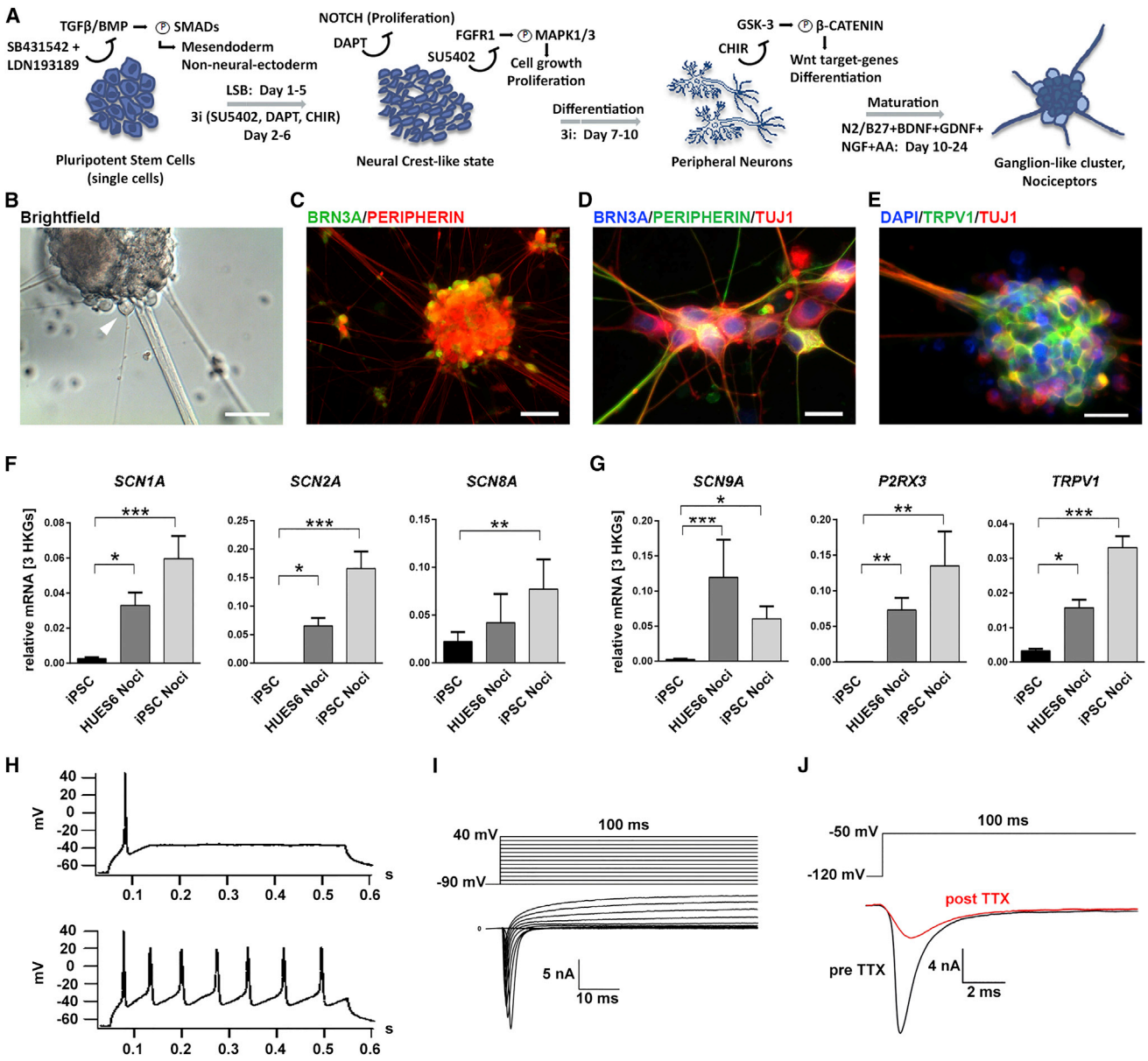

Figure 1. Differentiation of hPSCs into Human Nociceptors

(A) Overview of differentiation of human ESCs/iPSCs to nociceptors by LSB + 3i. L = LDN193189; SB = SB431542; 3i = DAPT, SU5402, CHIR99021.

(B) Bright-field image of a ganglion-like cluster. A nociceptor suitable for patch-clamp experiments is indicated by arrowhead.

(C) Ganglion-like clusters stain for BRN3A (green) and PERIPHERIN (red).

(D) Most cells in clusters co-express β3-TUBULIN (TUJ1, red), PERIPHERIN (green), and BRN3A (blue).

(E) Eighty-three percent of TUJ1-positive cells in clusters also express TRPV1.

(B–E) Scale bars represent 100 μm (B and C), 25 μm (D), and 20 μm (E).

(F and G) mRNA expression levels of neuronal NAVs (F) ($n \geq 4$ independent experiments, measured as duplicates) and of typical nociceptor ion channels (G) ($n \geq 4$ independent experiments, measured as duplicates). Error bars indicate the SEM.

(H–J) Functional characterization of hiPSC-derived nociceptors. (H) Current clamp recordings of representative phasically firing (top) and repetitively firing (bottom) nociceptors, elicited by injection of 100 pA for 500 ms. (I) Representative traces recorded with the indicated protocol (top) show sodium and potassium currents (bottom). (J) Example trace of voltage clamp recordings before and after addition of 500 nM TTX to the recording solution.

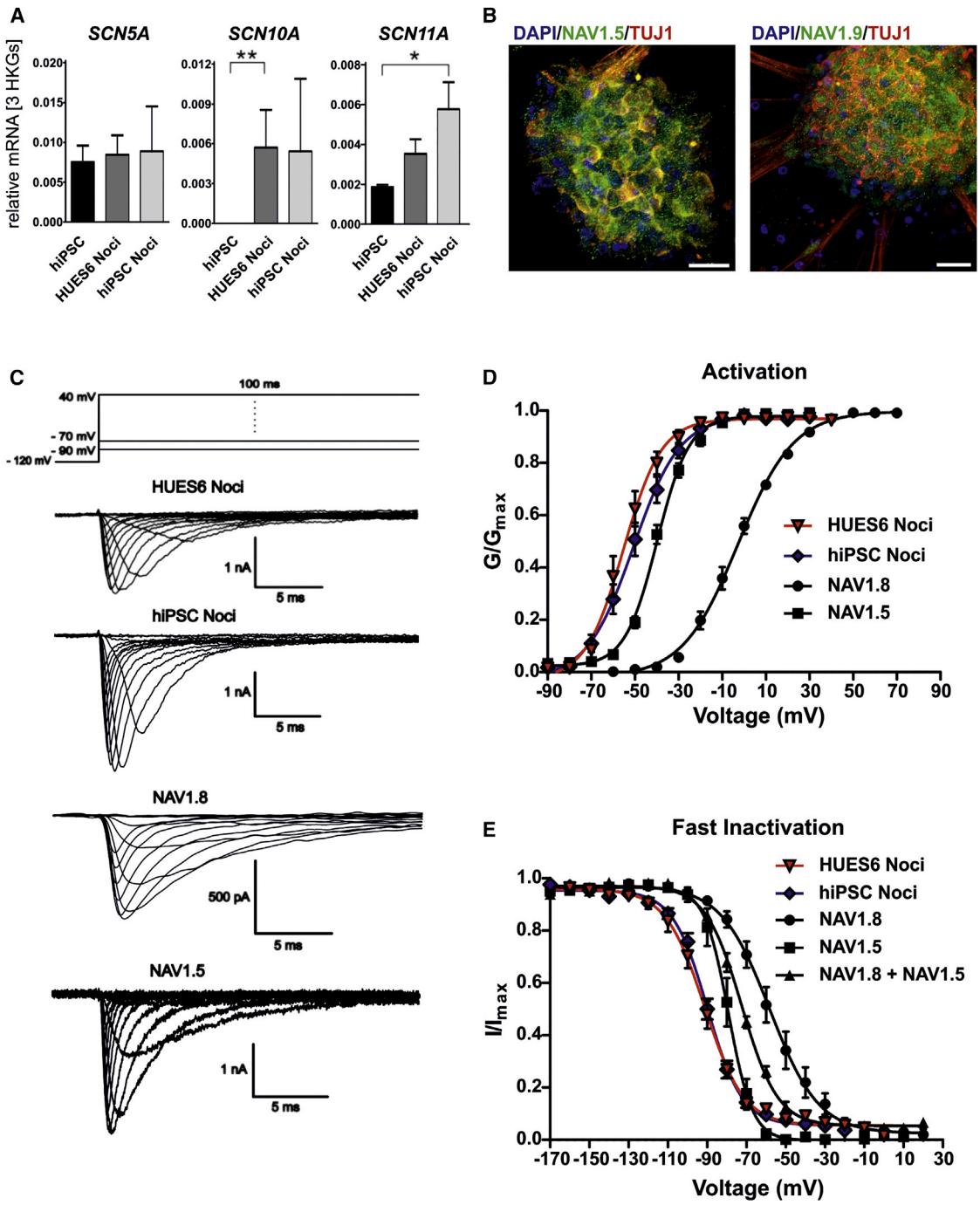

Figure 2. hPSC-Derived Human Nociceptors Express Three Types of TTXr NAVs

(A) mRNA levels of *SCN5A*, *SCN10A*, and *SCN11A* in hPSC-derived nociceptors in comparison to undifferentiated hiPSCs ($n \geq 4$ independent experiments, measured as duplicates).

(B) Immunofluorescence analysis of hiPSC-derived nociceptors revealed a dotted staining pattern for NAV1.5 and NAV1.9 (scale bars represent 20 μm).

(C) Top: schematic voltage protocol for recording of voltage-gated sodium currents. Bottom: representative traces of voltage clamp recordings of HUES6- and hiPSC-derived nociceptors and of heterologously expressed human NAV1.8 and NAV1.5.

(legend continued on next page)

expressed NAV1.5 than to that of NAV1.8 (Figure 2D; Table S1).

We focused on fast-inactivation properties, as these are very distinct between NAV1.5 and NAV1.8 in heterologous expression systems. As demonstrated in Figure 2E, the voltage dependence of steady-state fast inactivation of hPSC-derived nociceptors was hyperpolarized compared with NAV1.8, and rather in the range of that of NAV1.5.

Nevertheless, V_{half} of fast inactivation of TTXr currents from hPSC-derived nociceptors was more hyperpolarized than that of NAV1.5 alone in heterologous systems (Table S1). This may be due to either the expression of NAV1.9, or to the cellular background, which was shown to differentially affect gating of human NAVs (e.g., Rush et al., 2006).

hPSC-Derived Nociceptors Exhibit an Embryonic-like Expression Pattern of TTXr NAVs

Our results show that hPSC-derived nociceptors express an electrophysiologically relevant level of functional NAV1.5. Rat DRGs are well studied and available for comparison of the expression patterns of TTXr NAVs during development. Thus, we performed qRT-PCR experiments on E14–E16 and P6 rat DRGs. *Scn5a* was strongly expressed at E14–E16, but its expression levels declined after birth as expected (Figure 3A) (Renganathan et al., 2002). mRNA levels of *Scn9a* and *Scn10a* did not change significantly, whereas *Scn11a* was strongly upregulated after birth (Figure 3A). Whole-cell recordings showed fast-activating and -inactivating currents in DRGs from both E14–E16 and P6 rats, although current density was significantly lower in E14–E16 cells (E14–E16 cells: 104.4 ± 29.4 pF, n = 4; P6 cells: 196.2 ± 39.8 pA/pF, n = 21; compare scale bars in Figure 3B). Voltage dependence of activation of hPSC-derived nociceptors was more hyperpolarized than that of rat DRGs at both developmental stages (Figure 3C).

V_{half} of inactivation of all nociceptors was more negative than that of TTXr currents from P6 DRGs and much closer to that of E14–E16 DRGs, suggesting that the NAV subtype expression may be similar to developing sensory neurons. Fast inactivation of TTXr currents from E14–E16 DRGs showed two components (Figure 3D), reflecting the expression of more than one NAV subtype, probably including NAV1.5. In heterologous expression systems, NAV1.5 shows hyperpolarized fast inactivation compared with NAV1.8 (Figure 2E). Nevertheless, V_{half} of TTXr fast inactivation in human nociceptors (−93.0 ± 2.3 mV; −90,7 ± 1.6 mV for HUES6- and hiPSC-derived nociceptors, respectively) is still more hyperpolarized than that of NAV1.5 expressed in ND7/23 cells (−79.9 ± 2.4 mV). Also, the activation V_{half}s differ. This may be due to a differential regulation of NAV1.5 in human nociceptors compared with heterologous expression systems.

NAV1.5 is less resistant to TTX than NAV1.8 (IC_{50} for NAV1.5: 1–6 μM, for NAV1.8: 46 ± 10 μM; Renganathan et al., 2002). We took advantage of these diverse resistances to isolate the NAV1.5 current component from NAV1.8 and NAV1.9. Five μM TTX blocked heterologously expressed NAV1.5 by more than 65% (67% ± 3.6%), a concentration at which NAV1.8 was only blocked by 13.1% ± 2.7% (Figures 4A and 4B). The unblocked current fractions for hPSC-derived nociceptors were 42.5% ± 3.5% and 43.0% ± 1.5% (hiPSC- and HUES6-derived nociceptors, respectively), very similar to our results for NAV1.5 in heterologous expression systems (33% ± 3.6%; Figures 4B and 4C). These results confirm that our hPSC-derived nociceptors express a substantial level of functional NAV1.5.

NAV1.8 is supposed to support higher-frequency firing (Blair and Bean, 2002), especially due to its more depolarized fast-inactivation properties. TTXr fast inactivation is enhanced in the human nociceptors investigated here, suggesting that the firing rate may be reduced compared with mature healthy neurons. It is possible that this prevents nociceptive malfunction during development and supports normal development. Mutations in NAVs may interfere with this regulation and cause pain syndromes, such as PEPD, having its onset sometimes already in utero (Lampert et al., 2014). The model presented here offers a platform to investigate NAV physiology, and patient-derived nociceptors may be a useful tool to elucidate NAV dysfunction.

In summary, we successfully differentiated human sensory neurons from hPSCs. Our cells express canonical markers of nociceptors and exhibit many of their characteristic electrophysiological properties. hPSC-derived nociceptors have the potential to serve as a model system to interrogate the physiology and pharmacology of human TTXr NAVs, which emerged as prime targets for the development of new pain treatment.

We find that TTXr currents of these nociceptors are more similar to those of NAV1.5 than to those of NAV1.8 and NAV1.9, and the electrophysiological and pharmacological properties of NAV1.5, especially of fast inactivation, fit well to that of embryonic rodent DRGs. These data reveal that

(D and E) Voltage dependencies of activation (D) and steady-state fast inactivation (E) of HUES6-derived nociceptors (triangles, n = 15 cells of one experiment), hiPSC-derived nociceptors (diamonds, n = 23–26 cells), NAV1.8 (circles, n = 10–13 cells of one experiment), and NAV1.5 (squares, n = 8–10 cells of one experiment) and, shown only in (E), co-expression of NAV1.8 and NAV1.5 (triangles, n = 8 cells of one experiment).
All error bars indicate the SEM.

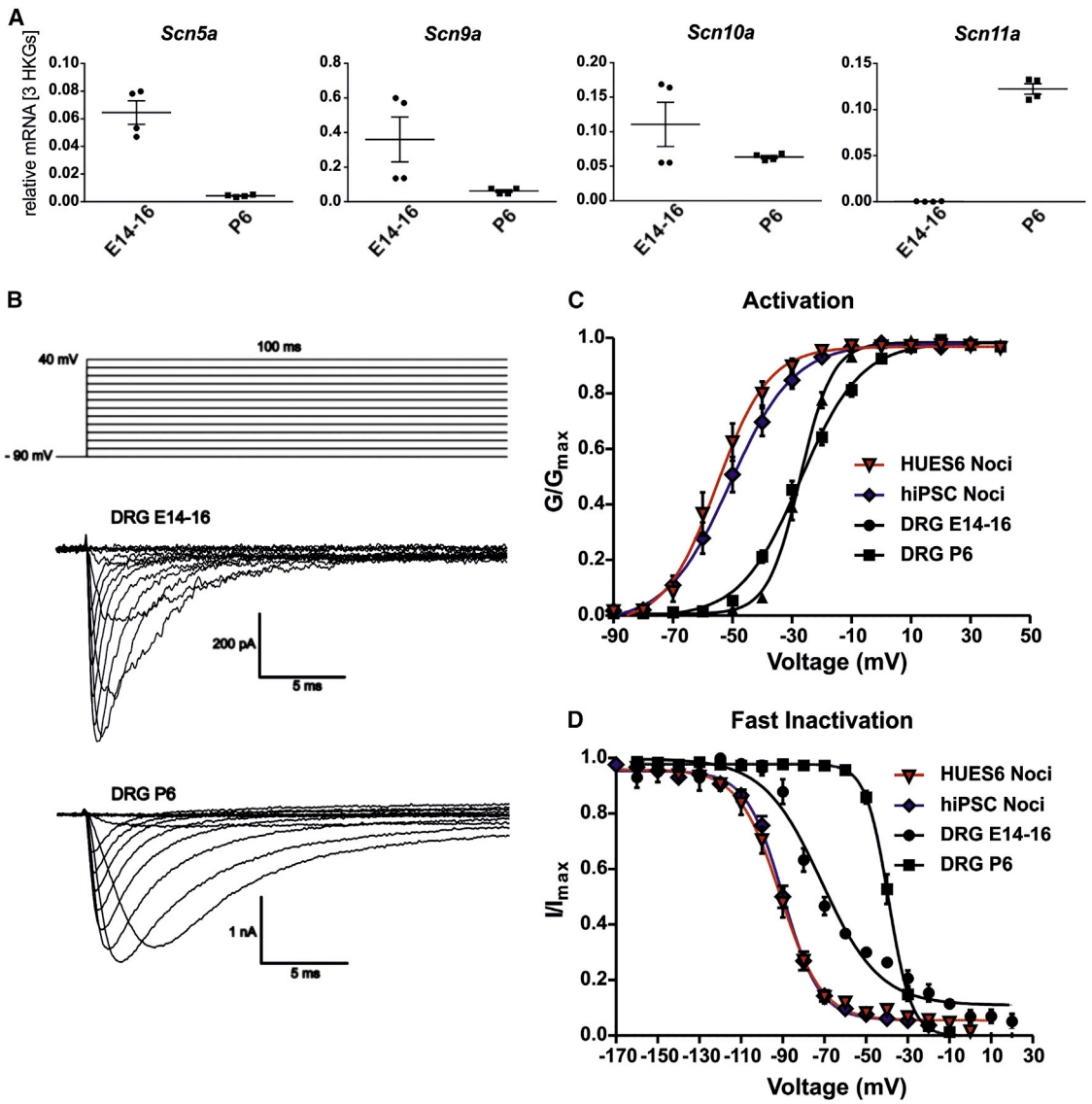

Figure 3. Expression of TTXr Sodium Channels in Developing rat DRGs

(A) mRNA expression levels of *Scn5a*, *Scn9a*, *Scn10a*, and *Scn11a* in DRGs of embryonic (E14–E16) and neonatal (P6) rats. *Scn5a* is downregulated and *Scn11a* upregulated (in neonatal DRGs compared with E14–E16 (n = 4, two independent experiments, shown as technical duplicates).

(B) Bottom: representative traces of voltage clamp recordings of E14–E16 and P6 DRGs in the presence of 500 nM TTX. Top: voltage protocol.

(C) Voltage dependence of activation of HUES6-derived (triangles, red fits, n = 15) and hiPSC-derived nociceptors (diamonds, blue fits, n = 26) is shifted toward more hyperpolarized potentials compared with rat E14–E16 DRGs (circles, black fits, n = 13 cells) and P6 DRGs (squares, black fits, n = 21 cells).

(D) Voltage dependence of steady-state fast inactivation of HUES6-derived (n = 15) and hiPSC-derived nociceptors (n = 23) is shifted toward more hyperpolarized potentials compared with embryonic and neonatal rat DRGs (n = 4 of 19 cells). Data of HUES6- and hiPSC-derived nociceptors are the same as shown in Figure 2.

All error bars indicate the SEM.

hPSC-derived nociceptors offer a unique opportunity of modeling developing nociceptors and may mimic in particular early-onset pain syndromes.

The differentiation of hiPSCs gained from patients with pain syndromes using this chemical approach might be a promising tool for the investigation of the

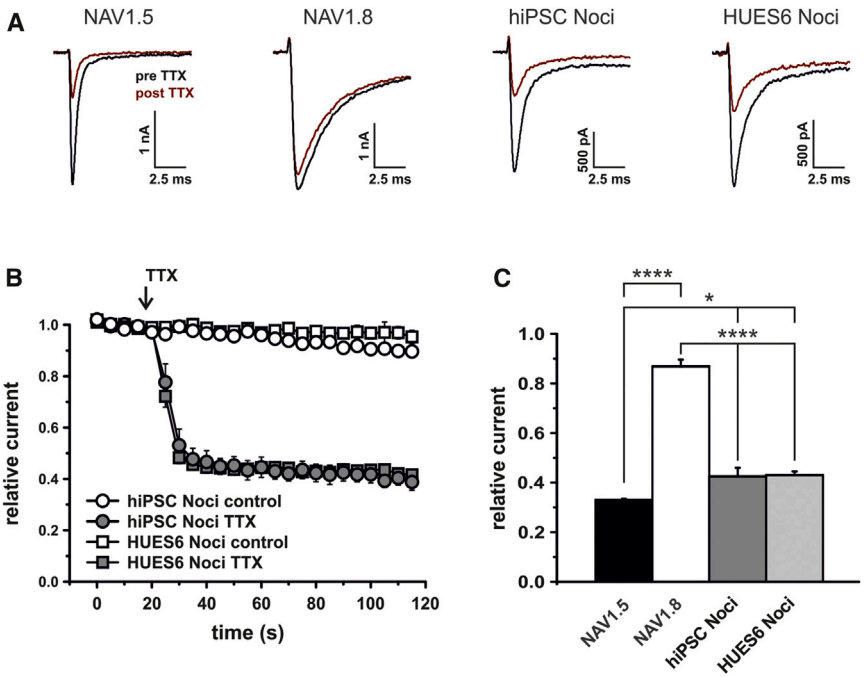

Figure 4. TTXr Currents in hPSC-Derived Nociceptors Display a NAV1.5-like TTX Sensitivity

(A) TTXr-current traces for human NAV1.5, NAV1.8, and hPSC-derived nociceptors prior to (black) and after (red) application of 5 μM TTX for 1 min. Note the slower current decay kinetics for NAV1.8.

(B) Relative TTXr currents measured during application of control or high-dose TTX (arrow, n = 3–5 cells).

(C) Relative remaining currents after application of 5 μM TTX for 1 min (n = 5–6 cells). All error bars indicate the SEM.

development of human sensory neurons carrying distinct mutations and thus may help to define druggable targets and to decipher the mechanisms underlying pain in humans.

EXPERIMENTAL PROCEDURES

Generation of Nociceptors from hiPSCs and hESCs

Following Institutional Review Board approval (Nr. 4120: "Generierung von humanen neuronalen Modellen bei neurodegenerativen Erkrankungen") and informed consent at the outpatient movement disorder clinic at the Department of Molecular Neurology, Universitätsklinikum Erlangen, Germany, hiPSCs were derived from a healthy Caucasian individual (previously referred to as Ctrl-1, Havlicek et al., 2014) with no history of neurologic disease. Fibroblasts isolated from dermal punch biopsies were reprogrammed by retroviral transduction with SOX2, KLF4 and c-MYC, and OCT3/4 (Takahashi et al., 2007) and were tested for pluripotency as described previously (Havlicek et al., 2014). All experiments with hESCs (HUES6) were carried out in accordance with the German Stem Cell Act (RKI AZ. 3.04.02/0069). hPSCs were cultured on Matrigel (BD Biosciences) in mTeSR1 medium (Stem Cell Technologies) and passaged in clumps.

Nociceptor differentiation was performed with modifications to Chambers et al. (2012). In brief, hPSCs were seeded as single cells at a density of 85,000–100,000 cells/cm^2 in presence of Y-27632 (Sigma-Aldrich). When cells reached 90%–100% confluence, dual SMAD inhibition was initiated by 100 nM LDN-193189 and 10 μM SB431542 on days 1–5.

Cells were fed daily, and N2/B27 medium (N2/B27 medium: DMEM/F12/Glutamax, with N2 and B27 [without VitA]; all LifeTechnologies) was added in increasing 25% increments every other day starting on day 4. Three μM CHIR99021, 10 μM SU5402, and 10 μM DAPT were added on days 2–10. On day 10, cells were dissociated using TrypLE Express (LifeTechnologies) and seeded on glass coverslips precoated with polyornithine/laminin (LifeTechnologies) or poly-D-lysine (Sigma-Aldrich). Long-term neuronal culture medium consisted of N2/B27 medium containing adjusted growth factor concentrations of 20 ng/ml human-b-NGF (beta nerve growth factor; R&D Systems), BDNF (brain derived neurotrophic factor), GDNF (glial-cell-line-derived neurotrophic factor; both Peprotech), and addition of 200 ng/ml ascorbic acid (Sigma-Aldrich).

Animals and DRG Culture

All animal experiments were performed in accordance with ethical guidelines established by German animal protection law approved by the animal protection committee of Regierung Mittelfranken, Germany. Embryos were removed from Wistar rats sacrificed at days 14–16 of pregnancy. DRGs were isolated from the embryos or the P6 rats and pooled into groups for RNA extraction and cell preparation (as described in Klinger et al., 2012). Cells were loaded on poly-D-lysine-coated glass coverslips, and experiments were performed the following day.

Culture of Cell Lines and Transfection of ND7/23 Cells

ND7/23 cells were maintained in DMEM (LifeTechnologies), including 10% fetal bovine serum (FBS), 4.5 g/L glucose, and 1% penicillin/streptomycin (PAA Laboratories) and transfected with human NAV1.5-cDNA, NAV1.8-cDNA, or both and GFP, using Nanofectin transfection reagent (PAA Laboratories). For the stable NAV1.5-HEK293 cell line, 30 g/ml Zeocin (Biochrom) was added, and glucose was reduced to 1 g/L.

qRT-PCR

RNA from DRGs and hPSC-derived nociceptors cultures was extracted and reversely transcribed, and PCRs were performed as previously described, using an Eppendorf realplex4 cycler (Eppendorf; Havlicek et al., 2014) and exon-spanning primers shown in Table S2. Differences in expression levels were determined by the ΔCq method.

Immunofluorescence Stainings

Immunofluorescence stainings were performed as described previously (Havlicek et al., 2014). Primary antibodies: anti-PERIPHERIN (C-19; 1:200; catalog number: SC-7604; Santa Cruz Biotechnology), anti-BRN3A (1:200; catalog number: AB5945; Merck Millipore), anti-TUBULIN (TUJ; 1:300; catalog number: MAB1864; Merck Millipore), anti-NAV1.5 (1:200; catalog number: ASC-013), anti-NAV1.9 (1:500; catalog number: ASC-017), and anti-TRPV1 (1:200; catalog number: ACC-030; all Alomone Labs). Images were acquired using a fluorescence or confocal microscope (Axio Observer.Z1, Carl Zeiss Microscopy).

Patch-Clamp Experiments of hPSC-Derived Nociceptors and DRG Cultures

Whole-cell recordings were performed with a HEKA EPC-10USB amplifier (HEKA electronics) using the following bath solution for voltage clamp: 140 mM NaCl, 1 mM $CaCl_2$, 1 mM $MgCl_2$, 10 mM HEPES, 20 mM TEA-Cl, 1 mM 4-Aminopyridin, 0.1 mM $CdCl_2$, and 10 mM D-glucose (pH 7.4). Glass electrodes (2.0–3.5 MΩ) were filled with solution containing 10 mM NaCl, 140 mM CsF, 10 mM HEPES, 1 mM EGTA, 5 mM D-glucose, and 5 mM TEA-Cl (pH 7.3). For voltage clamp recordings of DRGs, extracellular Na^+ was reduced (40 mM NaCl, 75 mM Cholin-Cl), and the internal solution contained 10 mM NaCl, 140 mM CsF, 10 mM HEPES, 1 mM EGTA, 15 mM D-glucose, and 10 mM TEA-Cl (pH 7.3).

For current clamp experiments the external solution contained 140 mM NaCl, 3 mM KCl, 1 mM $CaCl_2$, 1 mM $MgCl_2$, and 10 mM HEPES, (pH 7.4), and internal the solution contained 4 mM NaCl, 135 mM K-gluconate, 3 mM $MgCl_2$, 5 mM EGTA, 5 mM HEPES, 2 mM Na_2-ATP, and 0.3 mM Na_3-GTP (pH 7.25).

TTX (BIOTREND chemicals) was applied via a gravity-driven perfusion system or directly added to the bath solution prior to experiments. Capacitive transients were compensated for and leak (P/4) corrected for using the PatchMaster software (HEKA).

One hundred ms voltage pulses from a holding potential of −120 mV (for nociceptors) or −90 mV (for rat DRGs) to a range of potentials in 10 mV steps every 5 s were used to generate current-voltage (I-V) curves, which were fitted with a Boltzmann equation: $G_{Na} = G_{Na,max} / 1 + \exp [(Vm - V_{half}) / k]$, where G_{Na} is the sodium conductance, $G_{Na,max}$ is the maximal sodium conductance, V_{half} is the potential at which activation is half maximal, and k is the slope factor.

Voltage dependence of steady-state fast inactivation was assessed by 500 ms steps to various potentials in 10 mV increments followed by a test pulse to 20 mV to assess available channels.

Patch-Clamp Experiments on Cell Lines and Transfected Cells

Cell lines transiently expressing human NAV1.5, NAV1.8, or a combination of both were patch-clamped using an EPC-10USB or an Axopatch 200B amplifier and pClamp software (Axon Instruments). Holding potential was −120 mV. The external solution contained 140 mM NaCl, 3 mM KCl, 1 mM $CaCl_2$, 1 mM $MgCl_2$, 10 mM HEPES, and 10–20 mM D-glucose (pH 7.4). Internal solution contained 140 mM CsF, 10 mM NaCl, 10 mM HEPES, 1 mM EGTA, and 15 mM D-glucose (pH 7.38). External NaCl was reduced for recordings of the stable NAV1.5-HEK293 cell line: 70 mM NaCl, 70 mM Cholin-Cl, 3 mM KCl, 1 mM $CaCl_2$, 1 mM $MgCl_2$, 10 mM HEPES, and 20 mM D-glucose (pH 7.4). Internal NaCl was reduced to 2 mM, and TEA-Cl 10 mM was added to the pipette solution to improve recording conditions for NAV1.8 in ND7/23 cells.

For TTXr-current isolation, the bath solutions were supplemented with 500 nM TTX (control) or 5 μM TTX and continuously superfused during repetitive pulses to 20 mV every 5 s. Currents were normalized to the mean of the first four test pulses.

All patch-clamp recordings were performed at room temperature.

Statistics

Statistical analyses were performed in GraphPad Prism version 5.00 or Origin 8.6. Two groups were compared with one-tailed or two-tailed t tests. Kruskal-Wallis/One-Way ANOVA followed by Dunn's or Tukey multiple comparison tests were used when three or more groups were compared. p values < 0.05 were considered significant and are indicated as follows: * $p < 0.05$, ** $p < 0.01$, and ****$p < 0.0001$. All data are shown as mean ± SEM unless otherwise stated.

SUPPLEMENTAL INFORMATION

Supplemental Information includes two tables and can be found with this article online at http://dx.doi.org/10.1016/j.stemcr.2015.07.010.

AUTHOR CONTRIBUTIONS

E.E., S.H., and D.S. designed and performed experiments, collected and analyzed data, interpreted results, and wrote the manuscript. A.S.L. designed, performed, and analyzed qRT-PCR experiments and critically revised the manuscript. C.S., M.H., A.M.K., and A.K. performed patch-clamp experiments and analyzed data. Z.K. obtained human fibroblast samples, maintained fibroblast culture, clinically characterized donor, interpreted the data. C.N., J.W., and J.S. discussed and interpreted the data. C.A. discussed findings and contributed to the writing of the manuscript. B.N. conceived the study, interpreted results, and planned the experiments. B.W. and A.L. conceived the study, planned the experiments, interpreted the data, and wrote the manuscript.

ACKNOWLEDGMENTS

This work was supported by the Johannes and Frieda Marohn-Foundation (Win/2012). Additional funding came from the German Federal Ministry of Education and Research (BMBF, 01GQ113 to B.W.), the Bavarian Ministry of Sciences, Research and the Arts in the framework of the Bavarian Molecular Biosystems Reseach Network (to B.W.) and the ForIPS network (to B.W., Z.K., J.W.), the Interdisciplinary Center for Clinical Research (University Hospital Erlangen to B.W.), the Bavarian Research Foundation (PIZ-180-10), the German-Israeli-Foundation (GIF,

1091-27.1/2010 to A.L.), and the German Research Association (DFG LA2740/2-1 to A.L., NA 970 1/1 to B.N., INST 90/675-1 FUGG to C.A.) and the Jürgen Manchot Stiftung (PhD fellowship to A.S.L.). The present work was performed in fulfillment of the requirements for obtaining the degree "Dr. med." (E.E.). We thank Holger Wend, Sonja Plötz, Iwona Izydorczyk, and Michaela Hellwig for excellent technical support.

Received: November 3, 2014
Revised: July 27, 2015
Accepted: July 29, 2015
Published: August 27, 2015

REFERENCES

Bagal, S.K., Chapman, M.L., Marron, B.E., Prime, R., Storer, R.I., and Swain, N.A. (2014). Recent progress in sodium channel modulators for pain. Bioorg. Med. Chem. Lett. *24*, 3690–3699.

Blair, N.T., and Bean, B.P. (2002). Roles of tetrodotoxin (TTX)-sensitive Na+ current, TTX-resistant Na+ current, and Ca2+ current in the action potentials of nociceptive sensory neurons. J. Neurosci. *22*, 10277–10290.

Catterall, W.A. (2012). Voltage-gated sodium channels at 60: structure, function and pathophysiology. J. Physiol. *590*, 2577–2589.

Catterall, W.A., Goldin, A.L., and Waxman, S.G. (2005). International Union of Pharmacology. XLVII. Nomenclature and structure-function relationships of voltage-gated sodium channels. Pharmacol. Rev. *57*, 397–409.

Chambers, S.M., Qi, Y., Mica, Y., Lee, G., Zhang, X.J., Niu, L., Bilsland, J., Cao, L., Stevens, E., Whiting, P., et al. (2012). Combined small-molecule inhibition accelerates developmental timing and converts human pluripotent stem cells into nociceptors. Nat. Biotechnol. *30*, 715–720.

Faber, C.G., Lauria, G., Merkies, I.S., Cheng, X., Han, C., Ahn, H.S., Persson, A.K., Hoeijmakers, J.G., Gerrits, M.M., Pierro, T., et al. (2012). Gain-of-function Nav1.8 mutations in painful neuropathy. Proc. Natl. Acad. Sci. USA *109*, 19444–19449.

Freisinger, W., Schatz, J., Ditting, T., Lampert, A., Heinlein, S., Lale, N., Schmieder, R., and Veelken, R. (2013). Sensory renal innervation: a kidney-specific firing activity due to a unique expression pattern of voltage-gated sodium channels? Am. J. Physiol. Renal Physiol. *304*, F491–F497.

Gage, F.H., and Temple, S. (2013). Neural stem cells: generating and regenerating the brain. Neuron *80*, 588–601.

Havlicek, S., Kohl, Z., Mishra, H.K., Prots, I., Eberhardt, E., Denguir, N., Wend, H., Plötz, S., Boyer, L., Marchetto, M.C., et al. (2014). Gene dosage-dependent rescue of HSP neurite defects in SPG4 patients' neurons. Hum. Mol. Genet. *23*, 2527–2541.

Klinger, A.B., Eberhardt, M., Link, A.S., Namer, B., Kutsche, L.K., Schuy, E.T., Sittl, R., Hoffmann, T., Alzheimer, C., Huth, T., et al. (2012). Sea-anemone toxin ATX-II elicits A-fiber-dependent pain and enhances resurgent and persistent sodium currents in large sensory neurons. Mol. Pain *8*, 69.

Lampert, A., Eberhardt, M., and Waxman, S.G. (2014). Altered sodium channel gating as molecular basis for pain: contribution of activation, inactivation, and resurgent currents. Handbook Exp. Pharmacol. *221*, 91–110.

Renganathan, M., Dib-Hajj, S., and Waxman, S.G. (2002). Na(v)1.5 underlies the 'third TTX-R sodium current' in rat small DRG neurons. Brain Res. Mol. Brain Res. *106*, 70–82.

Rush, A.M., Dib-Hajj, S.D., Liu, S., Cummins, T.R., Black, J.A., and Waxman, S.G. (2006). A single sodium channel mutation produces hyper- or hypoexcitability in different types of neurons. Proc. Natl. Acad. Sci. USA *103*, 8245–8250.

Takahashi, K., Tanabe, K., Ohnuki, M., Narita, M., Ichisaka, T., Tomoda, K., and Yamanaka, S. (2007). Induction of pluripotent stem cells from adult human fibroblasts by defined factors. Cell *131*, 861–872.

Young, G.T., Gutteridge, A., Fox, H.D.E., Wilbrey, A.L., Cao, L., Cho, L.T., Brown, A.R., Benn, C.L., Kammonen, L.R., Friedman, J.H., et al. (2014). Characterizing human stem cell-derived sensory neurons at the single-cell level reveals their ion channel expression and utility in pain research. Mol. Ther. *22*, 1530–1543.

Stem Cell Reports

Supplemental Information

Pattern of Functional TTX-Resistant Sodium Channels Reveals a Developmental Stage of Human iPSC- and ESC-Derived Nociceptors

Esther Eberhardt, Steven Havlicek, Diana Schmidt, Andrea S. Link, Cristian Neacsu, Zacharias Kohl, Martin Hampl, Andreas M. Kist, Alexandra Klinger, Carla Nau, Jürgen Schüttler, Christian Alzheimer, Jürgen Winkler, Barbara Namer, Beate Winner, and Angelika Lampert

Table S1

Results of Boltzmann Fits of voltage-dependence of activation and fast inactivation

Activation	HUES6 Noci	hiPSC Noci	NAV1.5	NAV1.8	NAV1.5/NAV1.8	E14-16	P6
Vhalf	-53,5 ± 2,5 mV	-49.5 ± 2.4 mV	-39.8 ± 1,0 mV	-2,1 ± 1,5 mV		-26,4 ± 1,2 mV	-27,0 ± 0,9 mV
slope	6.19 ± 0.60 mV	7.1 ± 0,43 mV	8.19 ± 0.88 mV	11.75 ± 0.54 mV		9,9 ± 0,36 mV	4,8 ± 0,27 mV
Fast Inactivation							
Vhalf	-93,0 ± 2,3 mV	-90,7 ± 1,6 mV	-79,9 ± 2,4 mV	-58,1 ± 3,7	-73,1 ± 1,1 mV	-70,7 ± 0,9 mV	-39,7 ± 1,1 mV
slope	9.98 ± 0.46 mV	9.9 ± 0,81 mV	5.52 ± 0.49 mV	11.05 ± 0.78 mV	9.79 ± 0.53 mV	14,4 ± 1,46 mV	4,9 ± 0,21 mV

Table S2

Primers used for amplification of human and rat genes

Genes	Accession number (NCBI) or citation	Primer
human genes		
SCN1A (NAV1.1)	Candenas et al., 2006	for: 5'-GAAGAACAGCCCGTAGTGGAA-3' rev: 5'-TTCAAATGCCAGAGCACCA-3'
SCN2A (NAV1.2)	Candenas et al., 2006	for: 5'-GAAGGCAAAGGGAAACTCTGG-3' rev: 5'-CAGTGAGACATCAACAATCAGGAAG-3'
SCN5A (NAV1.5)	Candenas et al., 2006	for: 5'-CCGCCATTTACACCTTTGAGT-3' rev: 5'-CGCTGAGGCAGAAGACTGTG-3'
SCN8A (NAV1.6)	NM_014191.3	for: 5'-ACAATGTTGGGGCAGGATAC-3' rev: 5'-GGTGAAGAAGGAGCCGAAG-3'
SCN9A (NAV1.7)	NM_002977.3	for: 5'-ACCTATCTCTGCTTCAAGTTGC-3' rev: 5'-TGGGCTGCTTGTCTACATTAAC-3'
SCN10A (NAV1.8)	NM_006514.2	for: 5'-CTGTCGATGTCTCGGCATTC-3' rev: 5'-TGGGCACTTCTGTTCAGACTC-3'
SCN11A no1 (NAV1.9)	NM_014139.2	for: 5'-GAAATGCTTACCTCGCTCTG-3' rev: 5'-GCTCTCAAACTCTGGCTGTTG-3'
P2RX3	NM_002559.3	for: 5'-TCCCCAGGCTACAACTTCAG-3' rev: 5'-TGTTGAACTTGCCAGCATTC-3'
TRPV1	NM_080704.3	for: 5'-GCACAGGAGAGCAAGAACATC-3' rev: 5'-GTCCAGTTCACCTCGTCCAC-3'
GAPDH	NM_002046.4	for: 5'-GTCGGAGTCAACGGATTTG-3' rev: 5'-TGGGTGGAATCATATTGGAAC-3'
HPRT1	NM_000194.2	for: 5'-CCTGGCGTCGTGATTAGTG-3' rev: 5'-TCCCATCTCCTTCATCACATC-3'
B2M	NM_004048.2	for: 5'-GAGGCTATCCAGCGTACTCC-3' rev: 5'-AATGTCGGATGGATGAAACC-3'

rat genes		
Scn5a (Nav1.5*)*	NM_013125.2	for: 5'-TCGAGACCATGTGGGACTG-3' rev: 5'-AGCAAGGCCAAGAAGAGATTC-3'
Scn9a (Nav1.7)	NM_133289	for: 5'-CTTGGAGGGATCCAAAGATG-3' rev: 5'-TTTCTGCCAGCCTTCACAC-3'
Scn10a (Nav1.8)	NM_017247.1	for: 5'-AACGAACCTTTCCGAGCAC-3' rev: 5'-GGTGGGCACTTCAGCTTAG-3'
Scn11a (Nav1.9)	NM_019265.2	for: 5'-GGCAGCCAAGTCAATCTTTC-3' rev: 5'-TGAGGACCATCACGTCTACC-3'
Gapdh	NM_017008.4	for: 5'-CCTGGAGAAACCTGCCAAG-3' rev: 5'-CCCAGGATGCCCTTTAGTG-3'
Hprt1	NM_012583.2	for: 5'-TCCCAGCGTCGTGATTAG-3' rev: 5'-TCGAGCAAGTCTTTCAGTCC-3'
B2m	NM_012512.2	for: 5'-GTGCTTGCCATTCAGAAAAC-3' rev: 5'-AGTTGAGGAAGTTGGGCTTC-3'

Supplemental References

Candenas, L., M. Seda, P. Noheda, H. Buschmann, C. G. Cintado, J. D. Martin and F. M. Pinto (2006). "Molecular diversity of voltage-gated sodium channel alpha and beta subunit mRNAs in human tissues." Eur J Pharmacol **541**(1-2): 9-16.